



Discovery of a Young, Highly Scattered Pulsar PSR J1032-5804 with the Australian Square Kilometre Array Pathfinder

Ziteng Wang¹ , David L. Kaplan² , Rahul Sengar² , Emil Lenc³ , Andrew Zic³ , Akash Anumalapati² ,
B. M. Gaensler^{4,5,6} , Natasha Hurley-Walker¹ , Tara Murphy^{7,8} , and Yuanming Wang^{8,9}

¹ International Centre for Radio Astronomy Research, Curtin University, Bentley, WA 6102, Australia; ziteng.wang@curtin.edu.au

² Center for Gravitation, Cosmology, and Astrophysics, Department of Physics, University of Wisconsin-Milwaukee, P.O. Box 413, Milwaukee, WI 53201, USA

³ ATNF, CSIRO Space and Astronomy, P.O. Box 76, Epping, New South Wales 1710, Australia

⁴ Dunlap Institute for Astronomy and Astrophysics, University of Toronto, 50 St. George St., Toronto, ON, M5S 3H4, Canada

⁵ David A. Dunlap Department of Astronomy and Astrophysics, University of Toronto, 50 St. George St., Toronto, ON, M5S 3H4, Canada

⁶ Division of Physical and Biological Sciences, University of California Santa Cruz, 1156 High Street, Santa Cruz, CA 95064, USA

⁷ Sydney Institute for Astronomy, School of Physics, University of Sydney, Sydney, New South Wales 2006, Australia

⁸ ARC Centre of Excellence for Gravitational Wave Discovery (OzGrav), Hawthorn, Victoria 3122, Australia

⁹ Centre for Astrophysics and Supercomputing, Swinburne University of Technology, Hawthorn, VIC 3122, Australia

Received 2023 October 13; revised 2023 November 20; accepted 2023 November 24; published 2024 January 24

Abstract

We report the discovery of a young, highly scattered pulsar in a search for highly circularly polarized radio sources as part of the Australian Square Kilometre Array Pathfinder Variables and Slow Transients survey. In follow-up observations with the Parkes radio telescope, Murriyang, we identified PSR J1032–5804 and measured a period of 78.7 ms, a dispersion measure of 819 ± 4 pc cm⁻³, a rotation measure of -2000 ± 1 rad m⁻², and a characteristic age of 34.6 kyr. We found a pulse scattering timescale at 3 GHz of ~ 22 ms, implying a timescale at 1 GHz of ~ 3845 ms, which is the third most scattered pulsar known and explains its nondetection in previous pulsar surveys. We discuss the identification of a possible pulsar wind nebula and supernova remnant in the pulsar’s local environment by analyzing the pulsar spectral energy distribution and the surrounding extended emission from multiwavelength images. Our result highlights the possibility of identifying extremely scattered pulsars from radio continuum images. Ongoing and future large-scale radio continuum surveys will offer us an unprecedented opportunity to find more extreme pulsars (e.g., highly scattered, highly intermittent, and highly accelerated), which will enhance our understanding of the characteristics of pulsars and the interstellar medium.

Unified Astronomy Thesaurus concepts: Neutron stars (1108); Galactic radio sources (571); Radio pulsars (1353); Interstellar scattering (854)

1. Introduction

When radio pulses from pulsars traverse the turbulent interstellar medium, multipath propagation leads to temporal and spatial scattering, which in turn smears out the pulse profile. Despite extensive pulsar-searching surveys spanning decades (e.g., Lyne et al. 1998; Manchester et al. 2001; Lorimer & Kramer 2012; Keith et al. 2010; Stovall et al. 2014; Keane et al. 2018), some highly scattered pulsars remain challenging to detect with traditional time-domain techniques. These pulsars are especially hard to detect at frequencies $\lesssim 1$ GHz, where the majority of pulsar surveys take place. The periodic signal is difficult (or impossible) to detect when the observed pulse profile width is comparable to the pulsar spin period. For a Kolmogorov distribution of interstellar medium inhomogeneities, the scattering timescale τ scales with frequency ν as $\tau \propto \nu^{-4.4}$ (e.g., Romani et al. 1986). Most of the pulsar-searching surveys are not sensitive to highly scattered pulsars, as they are performed at a relatively low frequency, such as the High Time Resolution Universe Pulsar Survey (Keith et al. 2010) at ~ 1.4 GHz, the Green Bank Northern Celestial Cap Pulsar Survey (Stovall et al. 2014) at 350 MHz, and the MPIfR–MeerKAT Galactic Plane Survey

(MMGPS; Padmanabh et al. 2023), currently at ~ 1.4 GHz (from 856 to 1712 MHz).

As a concrete example, the most scattered pulsar found to date, PSR J1813–1749, was first identified as a pulsar candidate as a TeV source (Aharonian et al. 2005, 2006), an X-ray source (Brogan et al. 2005; Ubertini et al. 2005), and a supernova remnant (SNR) association (Brogan et al. 2005). Gotthelf & Halpern (2009) measured the pulse period $P = 44.7$ ms in X-rays, while no radio pulsations were detected with the Green Bank Telescope (GBT) at 1.4 and 2 GHz (Halpern et al. 2012) or the Effelsberg Telescope at 1.4 GHz (Dzib et al. 2018), though radio interferometric observations did detect a variable point source at the pulsar position (Dzib et al. 2010, 2018). Radio pulsations were finally detected with the GBT at frequencies of 4.4–10.2 GHz (Camilo et al. 2021). The pulsar was detected with a high scattering timescale $\tau \approx 0.25$ s at 2 GHz, which explains the nondetection in the previous pulsar searches.

The special properties of pulsars can help in identifying pulsar candidates in radio continuum images (e.g., Sett et al. 2023). Pulsars typically have steeper spectra than most other radio source types, with spectral indices $\alpha < -1$, where $S_\nu \propto \nu^\alpha$ (e.g., Bates et al. 2013; Posselt et al. 2023). Selecting steep-spectrum radio sources has long been used to find new pulsar candidates and has successfully identified new pulsars, including the first detected millisecond pulsar (MSP; Backer et al. 1982).

Pulsars are also one of a few astronomical sources measured to be strongly polarized (e.g., Lorimer & Kramer 2012; Johnston & Kerr 2018), and in particular circularly polarized. This means searches in circular polarization are another method that can be used to find them in the image domain (e.g., Gaensler et al. 1998). For example, Lenc et al. (2018) conducted an all-sky circular polarization survey at 200 MHz with the Murchison Widefield Array (MWA; Bowman et al. 2013) and identified 33 known pulsars. Pritchard et al. (2021) performed a circular polarization survey with the Australian Square Kilometre Array Pathfinder (ASKAP; Johnston et al. 2008; Hotan et al. 2021) on the Rapid ASKAP Continuum Survey (RACS; McConnell et al. 2020) data and identified 37 known pulsars. In a similar search, Kaplan et al. (2019) serendipitously discovered a new MSP, PSR J1431–6328, by identifying circularly polarized sources with the ASKAP data. Recently, Sobey et al. (2022) have discovered two new pulsars, PSR J1049 + 5822 and PSR J1602 + 3901, with the Low-Frequency Array Two-meter Sky Survey (LoTSS) as part of the Targeted search using LoTSS images for polarized pulsars survey.

Finally, pulsars can show flux density variability due to, for example, pulse nulling (e.g., Backer 1970), pulse intermittency (e.g., Kramer et al. 2006), interstellar scintillation (e.g., Rickett 1970), and/or eclipsing by the companion (e.g., Broderick et al. 2016). Finding highly variable sources is another way to select pulsar candidates, but additional criteria (e.g., radio spectra, polarization, multiwavelength counterpart associations) are often applied to make the sample size manageable. For example, Wang et al. (2022) identified 27 highly variable point sources toward the Magellanic Clouds with ASKAP, including a new pulsar. The new pulsar was the only source that was circularly polarized but that did not have a multiwavelength counterpart. Dai et al. (2016) discussed the prospect of identifying pulsars in variance images. These image-domain techniques can help us discover pulsars located in previously poorly explored parameter spaces, such as pulsars with high dispersion measure (DM), extreme nulling behaviors, and/or highly scattered pulses.

In this paper, we present the discovery of a young, highly scattered pulsar with the circular polarization search technique based on the data from two ASKAP projects: the Variable and Slow Transients (VAST; Murphy et al. 2013, 2021) survey and the Evolutionary Map of the Universe (EMU; Norris et al. 2011, 2021) survey. We confirmed the nature of the source in a dedicated search with the Parkes radio telescope, Murriyang. In Section 2, we summarize the discovery observations for the new pulsar. Analysis of archival observations and follow-up observations are discussed in Section 3. In Section 4, we discuss the properties and the local environment of the pulsar. We also discuss the prospects for identifying new pulsars, especially highly scattered ones, through image-domain techniques. The conclusions of this work are presented in Section 5.

2. Source Discovery

2.1. ASKAP Discovery

As part of the VAST survey, we have been conducting ASKAP observations of the southern Galactic plane. VAST observed 41 Galactic fields covering $|b| < 6^\circ$ and $\delta < -10^\circ$, totaling 1260 deg², repeating each field, on average, every two weeks¹⁰

since 2022 November. Each observation had ~ 12 minutes integration at a central frequency of 888 MHz with a bandwidth of 288 MHz, achieving a typical sensitivity of 0.4 mJy beam⁻¹ for the fields covering the Galactic plane. All four instrumental polarization products (XX, XY, YX, and YY) were recorded to allow images to be made in four Stokes parameters (I , Q , U , and V). The data were processed offline using the ASKAPSOFT pipeline (Cornwell et al. 2011), from which we can get Stokes I/V images and catalogs. PKS B1934–638 was used for the flux scale and bandpass calibration, and self-calibration was applied to correct for phase variations during the observation. A detailed description of the data reduction is given by Murphy et al. (2021).

We conducted a search for highly circularly polarized sources in the VAST Galactic plane observations to identify interesting sources (also see Pritchard et al. 2021; Rose et al. 2023 for the results of other circular polarization searches with ASKAP data). Most of the detected sources were matched to known pulsars or stellar objects. We selected VAST J103250.4–580434 for further investigation, because no clear multiwavelength association was found. VAST J103250.4–580434 was first detected in a VAST observation on 2022 November 19 (Schedule Block 45739) with a Stokes I peak flux density of 4.16 ± 0.52 mJy beam⁻¹ and a fractional circular polarization of $-28.5\% \pm 5.0\%$: a higher magnitude than average for pulsars, but consistent with the population (Anumarlapudi et al. 2023). The broader search results will be presented in future work.

2.2. Murriyang Discovery

Motivated by the detection of circular polarization and lack of multiwavelength association, we conducted a follow-up observation of VAST J103250.4–580434 with the 64 m Parkes telescope, Murriyang, on 2023 February 24 (project code PX103) with the Ultra-Wideband Low (UWL) receiver (Hobbs et al. 2020), which provides a wide frequency coverage spanning 704–4032 MHz and has been pivotal in confirming pulsar candidates that are scarcely detectable below 1.4 GHz (Sengar et al. 2023). The data were recorded in 1 bit pulsar-searching mode (total intensity) with the MEDUSA backend. The observation was 2500 s with a 32 μ s time resolution and 62.5 kHz frequency resolution (2048 channels per 128 MHz subband).

The periodic search was carried out with PULSAR_MINER¹¹ (Ridolfi et al. 2021), an automated pulsar-searching pipeline based on PRESTO¹² (Ransom 2001). To run the search more efficiently, we divided the data into two segments (1250 s each) and only selected two groups of subbands (the bottom-band group from 832 to 1216 MHz, considering the steep spectral indices for the normal pulsar population, and the high-band group from 2624 to 3008 MHz, considering the potential high scattering and/or dispersion). The DM range that we searched was 2–1500 pc cm⁻³ with harmonic summing of 8 and no acceleration search applied. We only folded the candidates with a signal-to-noise ratio (S/N) threshold of 8. We identified a strong pulsar candidate, now called PSR J1032–5804, with a period of 78.72 ms and a DM of 867.8 pc cm⁻³ in the high-band-group data. There is no previously published pulsar at this position in the ATNF pulsar catalog (Manchester et al. 2005),

¹¹ https://github.com/alex88ridolfi/PULSAR_MINER

¹² <https://github.com/scottransom/presto>

¹⁰ ASKAP uses dynamic scheduling, so we cannot give an exact cadence.

nor is there any unpublished discovery in the Pulsar Survey Scraper¹³ (Kaplan 2022).

PSR J1032–5804 was measured to have a wide pulse profile, with a duty cycle $\sim 30\%$ at ~ 2.8 GHz (using the pulse width at 50% maximum). After the initial discovery, we also folded the data at frequencies ranging from 1216 to 1600 MHz (centered at 1408 MHz) and from 3648 to 4032 MHz (centered at 3840 MHz), respectively. We saw a clear periodic signal (25.5σ) from the data centered at ~ 3.8 GHz, but no signal from the data centered at ~ 1.4 GHz.

3. Follow-up Observations and Source Properties

3.1. Timing and Polarization

All timing observations were conducted at the Murriyang radio telescope using the UWL receiver and MEDUSA backend. Each observation was recorded in both fold and search mode with full Stokes parameters along with a noise diode observation. All data were coherently dedispersed at the best DM value we could measure at the time of the observation (821 pc cm^{-3}). The time resolution for each observation was $128 \mu\text{s}$, with a bandwidth of 0.5 MHz per channel. Prior to the timing analysis, observations were first cleaned using `clfd`.¹⁴ We also excised each observation affected by narrowband and impulsive radio frequency interference (RFI) using `pazi` of the PSRCHIVE package. Using the highest-S/N observation, we created a standard profile using `pas` from the PSRCHIVE package (Hotan et al. 2004). Note that the pulsar is not visible below 2.5 GHz, therefore the UWL frequency band from 704 to 2500 MHz was removed from the analysis. All observations of the pulsar taken on 11 epochs were frequency-scrunched to one subband and polarization-scrunched to total intensity for timing (polarization analysis was performed separately). We divided the data into one to four subintegrations, depending on their S/N. To generate the times of arrival (TOAs), we used `pat` from PSRCHIVE and employed the Fourier domain with Markov Chain Monte Carlo algorithm. In total, 26 TOAs were obtained over 11 epochs, and each TOA had an S/N greater than 15.

We fit the TOAs derived from the Parkes/Murriyang data in PINT (Luo et al. 2021), using only frequencies above 2.5 GHz. We were able to obtain a good timing solution connecting back to our discovery observation, as shown in Figure 1 and given in Table 1, without rejecting any TOAs from the solution. We initially fit only for the rotation frequency f , but then added the frequency derivative \dot{f} once it was warranted by the residuals; the position was held fixed at the position from Australian Telescope Compact Array (ATCA) imaging. We verified that this solution was robust and unique using the Algorithmic Pulsar Timing for Binaries (APT_B; Taylor et al. 2023), which identified the same solution as we did by hand as the only solution. This solution has a reduced χ^2 of 1.97, suggesting that the uncertainties may be slightly underestimated or that there is some timing noise present. Regardless, we leave the uncertainties in Table 1 as the unscaled values reported by PINT, but note that they too may be slightly underestimated. There is also a contribution to the uncertainties on f and \dot{f} from our uncertainties in the ATCA imaging position, which is not taken into account by PINT. Using Appendix A of Hartman et al. (2008), we find uncertainties of $6 \times 10^{-10} \text{ Hz}$ and

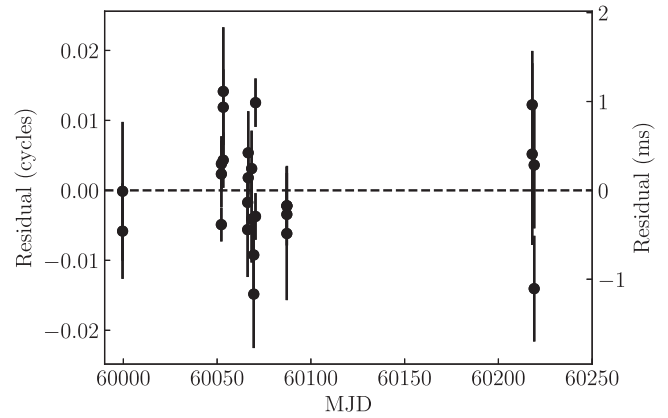


Figure 1. Timing residuals for PSR J1032–5804 from Parkes/Murriyang data. We plot the phase residuals (left y-axis) or time residuals (right y-axis) against the observation date (MJD).

Table 1
Measured and Derived Parameters for PSR J1032–5804

Parameter	Value
R.A. (J2000) ^a	$10^{\text{h}}32^{\text{m}}50^{\text{s}}.54(1)$
decl. (J2000) ^a	$-58^{\circ}04'34''.9(2)$
Start (MJD)	59999.6
End (MJD)	60219.1
Frequency (Hz)	$12.6998621581(4)$
Frequency Derivative (Hz s^{-1})	$-5.81654(10) \times 10^{-12}$
Epoch of Period (MJD)	60100
χ^2/dof	45.5/23
rms residual (μs)	504.7
DM (pc cm^{-3})	819 ± 4
RM (rad m^{-2})	-2000 ± 1
Galactic Longitude (deg)	285.436
Galactic Latitude (deg)	+0.008
Period (s)	$0.078741012111(2)$
Period Derivative (s s^{-1})	$3.60634(6) \times 10^{-14}$
Characteristic Age (kyr)	34.6
Surface Magnetic Field (G)	1.7×10^{12}
Spindown Luminosity (erg s^{-1})	2.9×10^{36}
Distance (kpc)	4.3^{b} $>50^{\text{c}}$

Notes. Quantities in parentheses are 1σ uncertainties on the last digit, without any additional scaling. The JPL DE405 solar system ephemeris has been used and times refer to TDB (using $\text{TT} = \text{TAI} + 32.184 \text{ s}$).

^a Derived from ATCA imaging.

^b From the Yao et al. (2017) electron density model.

^c From the Cordes & Lazio (2002) electron density model.

$1.3 \times 10^{-16} \text{ Hz s}^{-1}$ on f and \dot{f} from the position uncertainties, comparable to those from the timing analysis. In the future, once the data span exceeds 1 yr, we will be able to fit for a more precise timing position and reduce those uncertainties further.

We find that the pulsar is young, with a characteristic age of only 34.6 kyr. Given the modest time span of the current data, we cannot determine useful constraints on any higher timing derivatives. Allowing a fit for the second frequency derivative \ddot{f} finds $\ddot{f} = -(1.2 \pm 0.9) \times 10^{-22} \text{ Hz s}^{-2}$, consistent with 0, and implying a 3σ upper limit on the braking index of $n \equiv \ddot{f}/\dot{f}^2 < 102$. The distance to the pulsar is highly uncertain, with values from 4.3 kpc (YMW16 model; Yao et al. 2017) to >50 kpc (NE2001 model; Cordes & Lazio 2002), depending on the Galactic electron density model.

¹³ <https://pulsar.cgca-hub.org>

¹⁴ <https://github.com/v-morello/clfd>

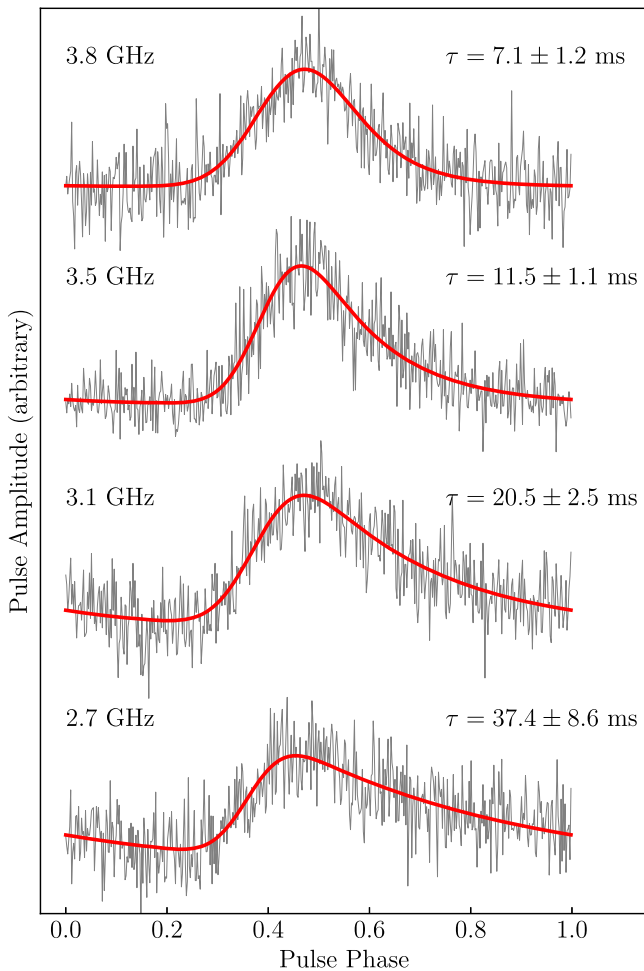


Figure 2. Normalized pulse profiles created from the summed Parkes UWL data of PSR J1032–5804 as a function of observing frequency. We show profiles (gray) at 3.8, 3.5, 3.1, and 2.7 GHz vertically offset from top to bottom, along with the best-fit exponential scattering model fits (red). The timescales for the scattering fits are given. A power-law fit to the frequency dependence of τ gives $\alpha_s = -4.7 \pm 0.7$ (with $\tau(\nu) \propto \nu^{\alpha_s}$) and a scattering timescale at 3 GHz of 22 ± 2 ms.

Once we had a timing solution, we coadded all of the available Parkes/Murriyang data into a single high-S/N data set. We then fit for an exponential scattering model (e.g., Lorimer & Kramer 2012). We assumed that the underlying profile model was a Gaussian and that scattering convolved this with a frequency-dependent exponential. Dividing up the data above 2.5 GHz into four subbands, we obtained the fits in Figure 2. The scattering timescale for each subband was fit independently: when we fit for a power-law frequency dependence, we obtain a spectral index $\alpha_s = -4.7 \pm 0.7$ (with $\tau(\nu) \propto \nu^{\alpha_s}$), consistent with expectations from Kolmogorov turbulence (Cordes et al. 1986; Romani et al. 1986; Cordes & Rickett 1998; Bhat et al. 2004) and a scattering timescale at 3 GHz of 22 ± 2 ms. The implied scattering timescale at 1 GHz was 3845 ms ($>40 \times$ the pulse period), a factor of 3 greater than that predicted by Bhat et al. (2004) based on the DM, a factor of 27 greater than that predicted by Lewandowski et al. (2015a), and a factor of 28 greater than that predicted by Yao et al. (2017).¹⁵ However, the scattering timescale of PSR J1032

¹⁵ The model of Cordes & Lazio (2002) is not sensible along this line of sight for $DM > 620 \text{ pc cm}^{-3}$.

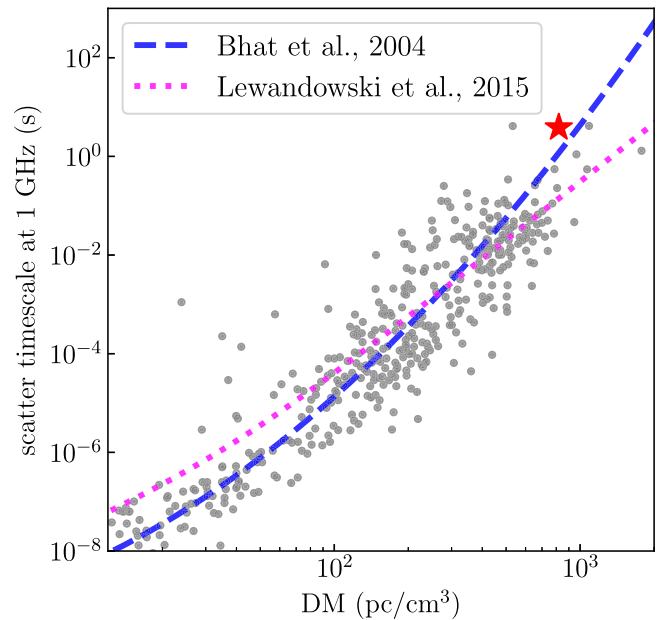


Figure 3. Scattering timescale as a function of the DM for PSR J1032–5804 (red star) and pulsars (gray dots) in the ATNF pulsar catalog (v. 1.70; Manchester et al. 2005). The dashed line corresponds to the scattering timescale and DM relation fitted by Bhat et al. (2004), while the dotted line corresponds to the one fitted by Lewandowski et al. (2015a).

–5804 is still largely consistent with the whole pulsar population (see Figure 3), considering the large internal uncertainties of these models.

Using the full Stokes fold mode (coherently dedispersed) UWL observations, we also conducted flux and polarization calibration. For polarization calibration, we used a short ~ 2 minutes observation of a linearly polarized noise diode, which was obtained at the start of each observing session. We used the radio galaxy PKS B0407–658 as a flux density reference, which is a more reliable calibration source for the UWL. Prior to performing any analysis, all observations were manually cleaned from RFI. For both polarimetric and flux calibration of the pulsar observations, we used PSRCHIVE’s `pac` pulsar archive calibration program, which was first used to generate a calibrator database. This database file was then used to obtain a flux- and polarization-calibrated file. This methodology of flux and polarization calibration is similar to the one outlined in Lower et al. (2020 and references therein).

We then used the `rmfit` tool of PSRCHIVE to fit for the rotation measure (RM) in one of the highest-S/N observations. We find a strong detection¹⁶ with $RM = -2000 \pm 1 \text{ rad m}^{-2}$. Though the RM measurement of PSR J1032–5804 is almost three times the most extreme $|RM|$ of known pulsars within 5° of PSR J1032–5804, the average interstellar magnetic field along the line of sight $B = 1.232 \text{ RM/DM} \approx -3 \mu\text{G}$ is consistent with the Galactic magnetic field model fitted by Han et al. (2018) and also with the Galactic pulsar distribution (see Figure 4). Based on the pulse profiles (see Figure 5), we find a circular polarization fraction of 10% at a frequency of 3 GHz, which is not consistent with the value of $\sim 25\%$ found from ASKAP imaging at 843 MHz. We also check the polarization evolution at three UWL frequencies (2.7, 3.2, and 3.8 GHz) and find that the circular polarization fraction remains similar

¹⁶ We used an RM search range between -3000 and 3000 rad m^{-2} to obtain the best `rmfit` value.

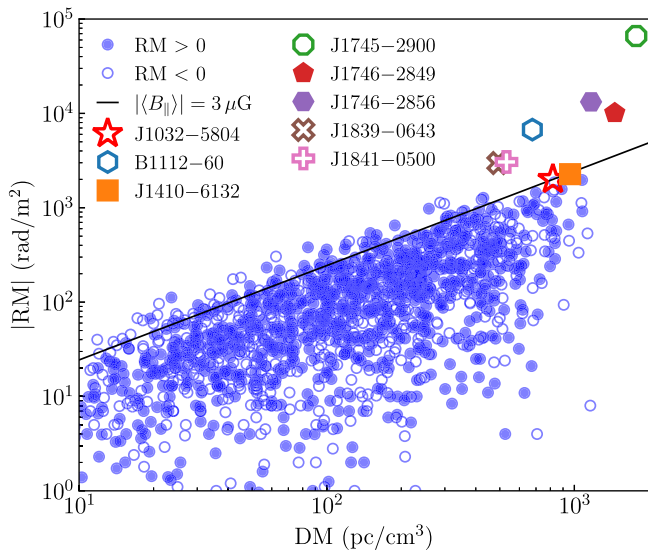


Figure 4. DM vs. RM for sources in the ATNF pulsar catalog (v. 1.70; Manchester et al. 2005). Sources with positive RM are filled, and those with negative RM are empty. Individual sources with $|RM| > 2000 \text{ rad m}^{-2}$ are labeled, and PSR J1032–5804 is the red star. We also plot a line indicating $|RM|/DM = 2.44 \text{ rad cm}^3 \text{ pc}^{-1} \text{ m}^{-2}$, corresponding to an average interstellar magnetic field along the line of sight of $3 \mu\text{G}$.

across these three UWL bands. However, we caution that the very broad pulse profile makes establishing a reliable pulse baseline—and therefore the total intensity pulsed flux density—difficult. We also find that there is very little position-angle change across the pulse, likely due to the long scattering timescale even at these frequencies (e.g., Li & Han 2003; Noutsos et al. 2015).

Apart from examining the highest-S/N observation, we also examined other observations taken at different epochs and found discrepancies in the RM values of up to 50 rad m^{-2} between them. These variations might resemble the changes in the magnetoionic conditions observed in pulsars within the Galactic Center (albeit on a smaller scale; Desvignes et al. 2018; Abbate et al. 2023) or elsewhere (Johnston et al. 2021). They could also be due to instrumental effects. Furthermore, different levels of RFI excision and changing S/Ns coupled with the highly scattered pulse profiles can potentially cause these discrepancies. Our ongoing investigation aims to ascertain whether these fluctuations stem from instrumental factors, to determine the time frame of these variations, and to establish any potential correlations with changes in DM. This comprehensive analysis is the subject of future work.

3.2. Radio Continuum

We looked at all available epochs of ASKAP data from VAST (22 observations so far) to probe the flux variability of PSR J1032–5804 (see Figure 6). We used forced flux measurements¹⁷ to deal with nondetections. Both the flux density and circular polarization fraction are consistent with no variability, with χ^2 of 14.7 for the flux density and 10.8 for the polarization fraction, both for 21 degrees of freedom (dof).

We also checked other ASKAP surveys from the CSIRO ASKAP Science Data Archive (CASDA). PSR J1032–5804 was detected in the RACS-mid survey (Duchesne et al. 2023)

¹⁷ We performed the fitting at the source position with the synthesized beam of that epoch.

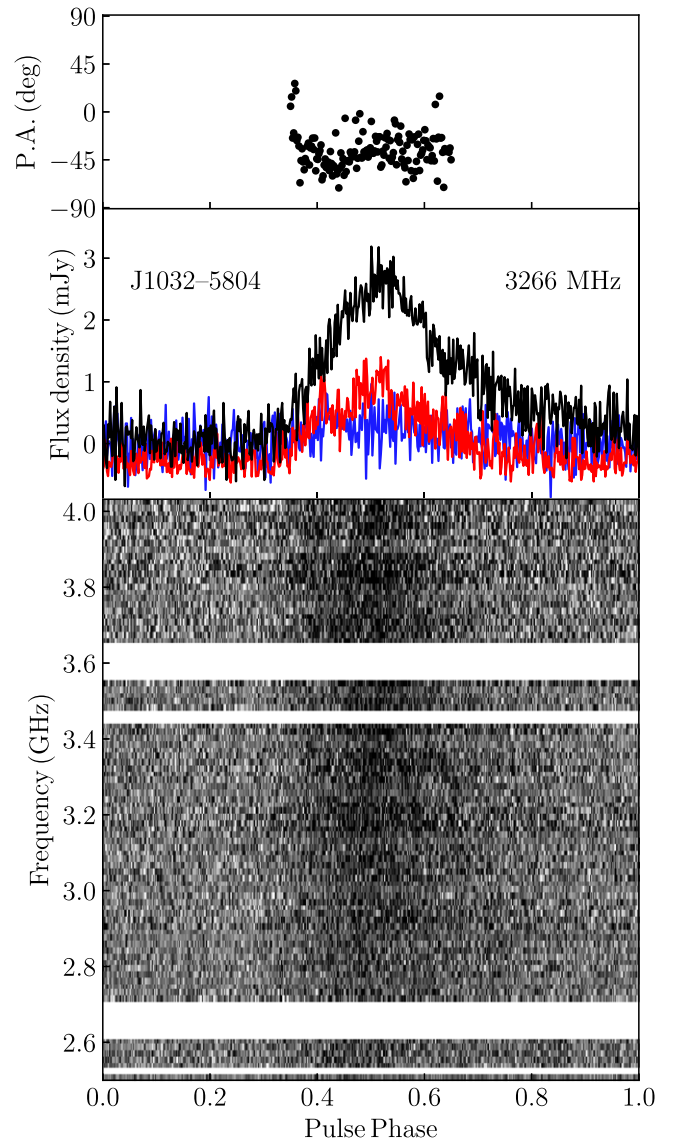


Figure 5. Dynamic spectra and polarization profiles of PSR J1032–5804 from a 52 minutes observation using the Parkes UWL receiver on 2023 May 2. The bottom panel shows the dynamic spectrum over the frequency range of 2.5–4 GHz in which pulsar is visible. The horizontal stripes correspond to the parts of the band that have been removed due to the presence of RFI. The middle panel shows the frequency-averaged profiles of the total intensity (in black), linear polarization (in red), and circular polarization (in blue). The top panel shows the polarization position angle (P.A.) at a central frequency of 3.25 GHz.

with a peak flux density of $2.84 \pm 0.38 \text{ mJy beam}^{-1}$ at 1367.5 MHz. It was also detected in the EMU (Norris et al. 2011, 2021) project with a peak flux density of $5.16 \pm 0.36 \text{ mJy beam}^{-1}$ and $4.96 \pm 0.37 \text{ mJy beam}^{-1}$ in the EMU fields 1017–60 (Schedule Block 46953) and 1029–55 (Schedule Block 46915) at 943.5 MHz, respectively.¹⁸

We also checked the GaLactic and Extragalactic All-sky MWA (GLEAM; Wayth et al. 2015; Hurley-Walker et al. 2017) survey data. There were no detections of the pulsar in any GLEAM bands, with a 3σ upper limit of $1.62 \text{ Jy beam}^{-1}$, $0.78 \text{ Jy beam}^{-1}$, $0.28 \text{ Jy beam}^{-1}$, and $0.14 \text{ Jy beam}^{-1}$ at 88 MHz, 118 MHz, 154 MHz, and 200 MHz, respectively. The elliptical

¹⁸ The EMU observations are typically ~ 10 hr, and the high flux uncertainties are mainly from the extended emission nearby.

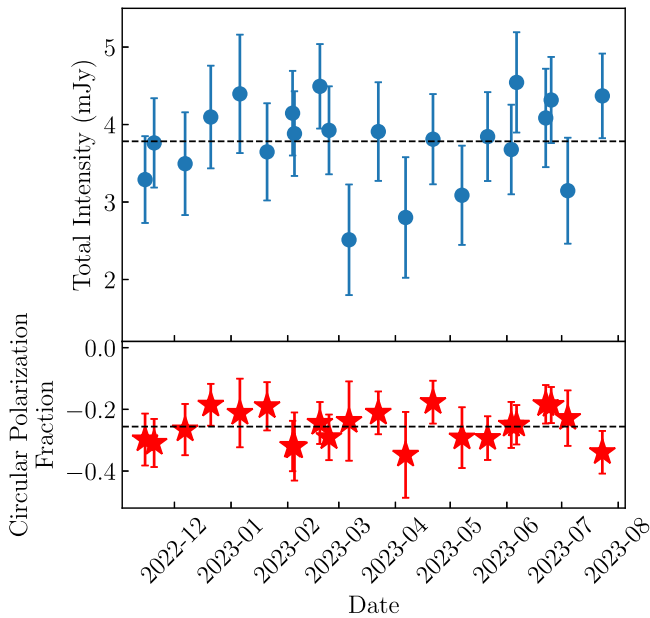


Figure 6. Total intensity (Stokes I) flux densities of PSR J1032–5804 from the VAST survey (top), along with circular polarization fractions (bottom). Both are consistent with constant values (dashed lines). We find a mean Stokes I flux density of 3.82 ± 0.13 mJy and a mean circular polarization fraction of -0.24 ± 0.02 .

structure in the ASKAP images is visible, albeit at low resolution and significance.

Unlike most pulsars whose radio spectra can be modeled by a simple power law (e.g., Bates et al. 2013), the spectrum of PSR J1032–5804 may peak at ~ 1 GHz and decline at higher and lower frequencies. To obtain the spectral energy distribution (SED) over a wide frequency range, we observed PSR J1032–5804 with ATCA on 2023 August 21 (project code C3363) with 6D configuration in the L (1–3 GHz) and C/X (5–7 GHz and 8–10 GHz) bands for 3 hr each. The observations were calibrated using PKS B1934–638 for the flux density scale and the instrumental bandpass. PMN J1047–6217 was used for phase calibration. We used CASA to perform both the data calibration and the continuum imaging. We split each band into two parts to image the data. We detected a compact radio source at the pulsar position in all six subbands (see Table 2). The best-fit position of PSR J1032–5804 from the ATCA observation (based on the X-band data) is R.A. $10^{\text{h}}32^{\text{m}}50^{\text{s}}54 \pm 0^{\text{s}}01$, decl. $-58^{\circ}04'34''9 \pm 0''2$, which is within the ASKAP 1σ positional error circle.

3.3. Swift X-Ray Observations

Motivated by the fact that PSR J1032–5804 seems to be young and energetic, we looked for available X-ray data, but there were no observations with Chandra or XMM-Newton that covered this location. There was one short observation with the Neil Gehrels Swift Observatory (Gehrels et al. 2004), but the duration was only 400 s. Therefore, we requested a longer Director’s Discretionary Time observation. We observed PSR J1032–5804 using the Swift X-ray Telescope (XRT; Burrows et al. 2005) for a total of 2242 s in two exposures on 2023 May 22 and 2023 May 26. We retrieved the merged data set created with the online analysis tools.¹⁹ We find zero events

Table 2
ATCA Flux Density Measurement for PSR J1032–5804

Frequency Range (MHz)	$S_{\text{Stokes } I}$ (mJy beam $^{-1}$)	$S_{\text{Stokes } V}$ (mJy beam $^{-1}$)
1076–2100	2.09 ± 0.64	-0.56 ± 0.07
2100–3124	1.76 ± 0.20	-0.19 ± 0.06
4476–5500	0.73 ± 0.04	<0.14
5500–6524	0.56 ± 0.05	<0.13
7976–9000	0.22 ± 0.03	<0.10
9000–10,024	0.19 ± 0.03	<0.12

Note. Nondetections are denoted by 3σ upper limits based on the local noise.

within $15''$ of PSR J1032–5804, and derive a 95% upper limit on the count rate of $5 \times 10^{-4} \text{ s}^{-1}$.

To interpret the X-ray upper limit, we first convert the DM into a hydrogen column density using the relationship of He et al. (2013) and find $N_{\text{H}} \approx 2.5 \times 10^{22} \text{ cm}^{-2}$. We assume a power-law X-ray spectrum with index $\Gamma = 1.5$, typical of young pulsars like PSR J1032–5804 (Helfand et al. 2007; Kargaltsev & Pavlov 2008; Kargaltsev et al. 2012, although Gotthelf 2003 would predict a flatter spectrum for this \dot{E}). This then gives an upper limit to the unabsorbed flux (0.5–8 keV) of $5.5 \times 10^{-14} \text{ erg cm}^{-2} \text{ s}^{-1}$, or an upper limit to the luminosity of $1.6 \times 10^{32} d_5^2 \text{ erg s}^{-1}$, where the distance is $5d_5$ kpc. We can compare this with the spindown luminosity and find $L_{\text{X}}/\dot{E} < 5 \times 10^{-5} d_5^2$. This is lower than many young pulsars, but not inconsistent with the tail of the population (Kargaltsev & Pavlov 2008; Kargaltsev et al. 2012). A deeper X-ray observation may be able to more robustly constrain any X-ray emission, although the highly uncertain distance will make any constraints somewhat weak.

4. Discussion

PSR J1032–5804 was detected as a point source in all ASKAP and ATCA observations. Despite the large scattering timescale, the angular broadening effect is small compared to the synthesized beam of all images. For a source at a distance d scattered by a single thin screen at a distance s , the expected FWHM of angular broadening follows

$$\theta = \sqrt{\frac{8 \ln 2c(d-s)\tau}{ds}},$$

where τ is the scattering timescale and c is the speed of light (Cordes & Lazio 1997). Assuming $d = 4.3$ kpc and $s = d/2$, the expected angular broadening is $\theta \approx 2'' (\nu/1 \text{ GHz})^{-2.2}$. All synthesized beam sizes are much larger than the expected value at corresponding frequencies (e.g., $\theta_{2.1 \text{ GHz}} \approx 0''4$, while the ATCA synthesized beam at 2.1 GHz is $\sim 5''$). The large scattering timescale also leads to low-level time variability in the image domain. Assuming a Kolmogorov spectrum (e.g., Rickett 1977), we calculated a diffractive scintillation bandwidth of $\Delta f_{\text{DISS}} \ll 1$ kHz and a scintillation timescale of $\ll 10$ s at 888 MHz. Both the scintillation bandwidth and the timescale are much smaller than those for typical VAST observations (288 MHz and 12 minutes), which could explain the nonvariability of the source in the VAST survey.

Motivated by the youth of PSR J1032–5804, we searched for an associated SNR. There are no cataloged SNRs coincident with the pulsar, with the closest $>1.5'$ away (Green 2019, 2022

¹⁹ https://www.swift.ac.uk/user_objects/

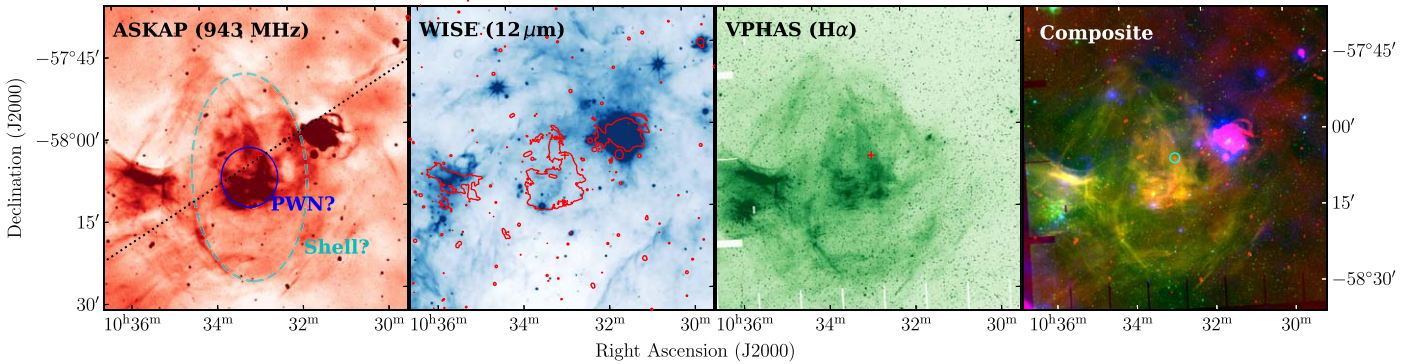


Figure 7. The field of PSR J1032–5804, observed with ASKAP at 943 MHz (from EMU; Norris et al. 2011; left), WISE (from the ALLWISE data release; Cutri et al. 2013) $12\ \mu\text{m}$ (middle left), and $\text{H}\alpha$ from VPHAS (Drew et al. 2014; middle right). All images are roughly $0\text{''}8$ on a side with north up. The position of PSR J1032–5804 is shown by the red plus. The Galactic plane is indicated with the black dotted line. On the ASKAP image, we show the outline of a potential SNR shell (cyan dashed ellipse) and a more compact PWN (magenta circle). On the WISE image, we also show contours from the ASKAP image (red). We also show a composite of radio (EMU; red), infrared (WISE; blue), and $\text{H}\alpha$ (VPHAS; green) emission (right), where the position of PSR J1032–5804 is shown by the cyan circle.

December version). We therefore examined deeper radio images from the EMU project.²⁰ The 10 hr EMU observation reaches a sensitivity of $28\ \mu\text{Jy beam}^{-1}$ with a resolution of 15'' . We retrieved EMU field 1017–60 from CASDA. Figure 7 shows a cutout of the region around PSR J1032–5804. There is a considerable amount of extended emission around the position of PSR J1032–5804 in the EMU image, with a potential SNR shell outlined in cyan and a more compact emission region (potentially a pulsar wind nebula or PWN) outlined in blue. However, we caution that there is a lot of other extended emission in this region and it is not confined to only the area around PSR J1032–5804, suggesting that there could be contributions from Galactic H II regions or unrelated synchrotron emission. Unfortunately, difficulties in robustly deconvolving the complex extended emission in this region prevent us from establishing a reliable in-band spectral index that might help discriminate between these sources of emission. Nor can we identify a radio image at another wavelength to do the same. Instead we examined the $12\ \mu\text{m}$ image from ALLWISE (Cutri et al. 2013). We also assembled an $\text{H}\alpha$ mosaic from six individual exposures from the Very Large Telescope Survey Telescope (VST) Photometric $\text{H}\alpha$ Survey (VPHAS; Drew et al. 2014), which we mosaicked together with `swarp` (Bertin et al. 2002) to remove the gaps between the individual detectors. These images are shown in Figure 7. Plotting the EMU contours on the ALLWISE image, we see that most of the radio emission is roughly traced by the $12\ \mu\text{m}$ emission, as expected for thermal bremsstrahlung emission from H II regions (e.g., Condon et al. 1999; Condon & Ransom 2016; Khan et al. 2022). However, the central emission closest to PSR J1032–5804, the putative PWN, does not show any emission at $12\ \mu\text{m}$. That region is bright in $\text{H}\alpha$, and there is also a good correspondence between the diffuse radio emission (putative PWN) surrounding PSR J1032–5804 and the diffuse $\text{H}\alpha$ emission, including narrow filaments (the putative shell). Other regions that are bright at $12\ \mu\text{m}$ are seen at radio and optical wavelengths, suggesting thermal emission, but the region surrounding the pulsar generally lacks mid-infrared emission. This suggests that it may in fact be nonthermal emission associated with PSR J1032–5804, but we will need better multiwavelength imaging (including

potentially deeper X-ray images) or optical spectroscopy to confirm this.

The SED of PSR J1032–5804 is shown in Figure 8 (we excluded GLEAM data points here, as they are not constraining). The SED is ambiguous and noisy: it may continue as a typical pulsar power law, but it also may peak at a frequency $\sim 1\ \text{GHz}$. This may be evidence of gigahertz-peaked spectrum (GPS) behavior. Previous studies have suggested that the origin of the gigahertz spectral turnover is likely caused by the absorption from the pulsar ambient environment, such as SNRs, PWNs, and H II regions (e.g., Kijak et al. 2011; Rajwade et al. 2016). In Figure 8, we fit the SED of PSR J1032–5804 with a simple power law and the thermal free–free absorption model described by Lewandowski et al. (2015b):

$$S(\nu) = S_1(\nu/1\ \text{GHz})^\alpha e^{-B\nu^{-2.1}},$$

where S_1 is the pulsar’s intrinsic flux density at 1 GHz, α is the pulsar’s intrinsic spectral index, and $B = 0.08235 \times T_e^{-1.35} \text{EM}$ (emission measure $\text{EM} = n_e^2 s$; n_e , s , and T_e are the absorbing material electron density, size, and electron temperature, respectively). For the power-law model, we found a spectral index of -1.13 ± 0.03 . For the absorption model, we estimated $S_1 = 9.61_{-1.19}^{+1.52}$, $\alpha = -1.66_{-0.08}^{+0.08}$, and $B = 0.86_{-0.12}^{+0.12}$, and found the peak frequency $\nu_p = 1.04\ \text{GHz}$. The peak frequency for PSR J1032–5804 is consistent with the known GPS pulsar population (see Figure 7 in Kijak et al. 2021). We also note that there are deviations from both the free–free absorption model and the power-law model. We compared these two models using the F -statistic (e.g., Weisberg 2005). The distribution of the F -statistic follows an F -distribution with $d_1 = 1$, $d_2 = 6$ dof. We calculated an F -statistic of 6.80 with a corresponding p -value of 0.04, which means that the free–free absorption model fits significantly better than the power-law model.

In Figure 9, we show the constraints on the electron density and temperature of the absorber based on the fitted parameters and consider three scenarios: a dense SNR filament (with $s = 0.1\ \text{pc}$), a PWN (with $s = 1.0\ \text{pc}$), and a cold H II region (with $s = 10.0\ \text{pc}$). The results are broadly consistent with either the SNR filament or the PWN scenario (see Kijak et al. 2021 and references therein), which agrees with the EMU extended emission analysis above. For both scenarios, the expected fractional DM contribution from the local

²⁰ The ATCA images from Section 3.2 were not useful in searching for extended emission because of limited uv coverage.

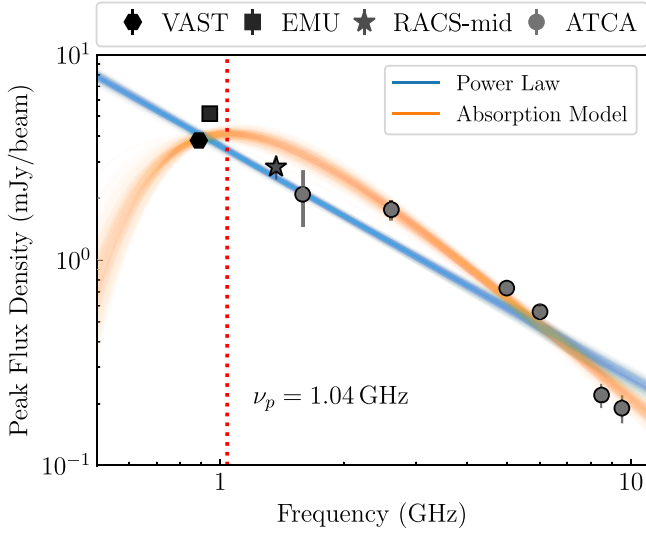


Figure 8. The radio spectrum of PSR J1032–5804. Besides the ATCA data listed in Table 2, we also used VAST, EMU, and RACS-mid data in this fit. For the surveys with multiple observations (VAST and EMU), we used the mean flux density mentioned in Section 3.2. The orange line shows the fitted free-free absorption model and the red dashed line shows the corresponding peak frequency, while the blue line shows the simple power-law fit with a spectrum index of -1.13 ± 0.03 .

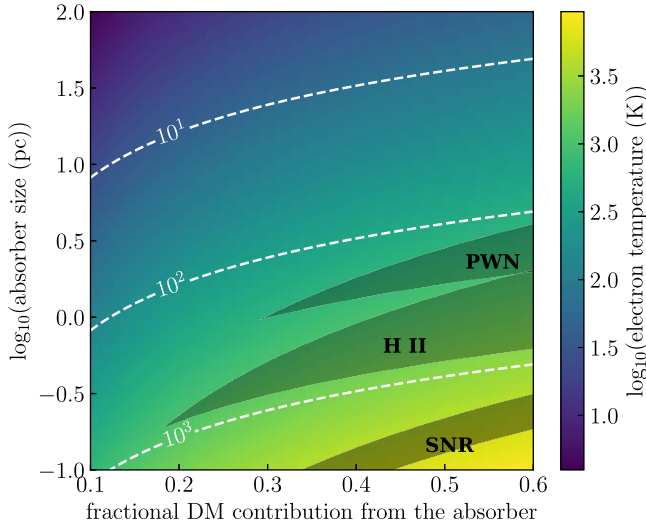


Figure 9. Constraints on the electron temperature T_e (white dashed lines) and electron density n_e (heat map) based on the best-fitted parameters (i.e., $B = 0.99$). The x -axis shows the fractional DM contribution from the absorber, and the y -axis shows the size of the absorber on a logarithmic scale. We show expected values for different absorbers in the shaded regions: (1) SNR filament with $n_e \gtrsim 10^3 \text{ cm}^{-3}$ and $T_e \sim 5000 \text{ K}$ (e.g., Lee et al. 2013); (2) PWN with $n_e \sim 50\text{--}250 \text{ cm}^{-3}$ and $T_e \sim 1500 \text{ K}$ (e.g., Gaensler & Slane 2006); and (3) H II region with $n_e \gtrsim 10^2 \text{ cm}^{-3}$ and $T_e \sim 1000\text{--}5000 \text{ K}$. (e.g., Shabala et al. 2006). The typical sizes of an SNR filament, PWN, and H II are 0.1 pc, 1 pc, and 10 pc, respectively. Assuming a free-free absorption model, our result largely agrees with the SNR filament or PWN scenario.

environment is around 50%, which could potentially break the inferences we made in previous discussions regarding the correlations between DM, RM, and the scattering timescale. For example, with a large DM contribution, the magnetic field of the local environment could dominate the RM value we measured, which could lead to a wrong estimation of the average interstellar magnetic field along the line of sight. The relation between scattering timescales and DMs could also be

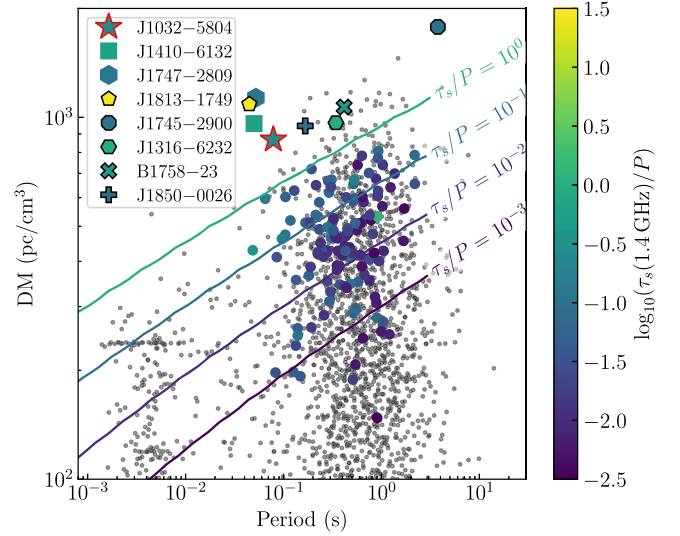


Figure 10. DM vs. pulse period P for sources in the ATNF pulsar catalog (v. 1.70). Pulsars without cataloged scattering timescales are shown as black points. Those with cataloged scattering timescales τ_s at 1.4 GHz are colored according to the ratio of the timescale divided by the pulse period, with the color bar shown on the right. We also plot contours of constant τ_s/P based on the model of Bhat et al. (2004). Sources with $\tau_s/P > 1$ should not be detectable as pulsed sources at 1.4 GHz. Individual highly scattered pulsars are labeled, with values for PSR J1410–6132 taken from O’Brien et al. (2008) and PSR J1747–2809 taken from Camilo et al. (2009). PSR J1032–5804 is the star with the red outline.

significantly affected if there are additional screens near the pulsar (e.g., Cordes et al. 2016).

Besides free-free absorption, synchrotron self-absorption in the pulsar magnetosphere (Sieber 1973) or flux dilution caused by anomalous scattering (Cordes & Lazio 2001; Dembska et al. 2014) can also lead to a decrease in the flux density at lower frequencies. Given that the data we have are all above $\sim 0.8 \text{ GHz}$, it is hard to get a robust constraint on the surrounding environment for PSR J1032–5804 without low-frequency observations. Further deep radio continuum observations (especially at lower frequencies) of the pulsar itself and the surrounding extended emission and/or deeper X-ray images may be helpful in understanding the nature of the pulsar spectrum and probing the interstellar medium in the pulsar’s local environment (e.g., a potential SNR association).

PSR J1032–5804 is the third most scattered pulsar known, which makes it hard to detect in periodicity searches. In Figure 10, we plot the DM versus period for the pulsars in the ATNF pulsar catalog (Manchester et al. 2005). In general, as DM increases, so does the scattering (Cordes & Lazio 2002; Bhat et al. 2004; Lewandowski et al. 2015a; Yao et al. 2017). Those sources with the highest DMs and the shortest periods will then be the hardest to detect in a pulsation search. This is illustrated not only by the case of PSR J1032–5804, but also by other similar sources, such as PSR J1813–1749 (Gotthelf & Halpern 2009; Dzib et al. 2010; Halpern et al. 2012; Camilo et al. 2021). While PSR J1813–1749 is even more scattered than PSR J1032–5804, both of them are undetectable as pulsed sources at the normal search frequency of 1.4 GHz. This is consistent with the fact that the location of PSR J1032–5804 was searched as part of the Parkes multibeam pulsar survey (Manchester et al. 2001) and the deeper High Time Resolution Universe midlatitude survey (Keith et al. 2010; Bates et al. 2011a), both centered at 1.4 GHz, but it was not identified.

Many previous pulsar surveys are not sensitive to the highly scattered short-period pulsars, as most of them were conducted at lower frequencies (ranging from ~ 300 to 1400 MHz). Searching for pulsars at high frequency is one of the ways to detect more new pulsars of this kind. However, only a few new pulsars have been discovered in previous very-high-frequency ($\nu \gtrsim 5$ GHz) pulsar surveys (e.g., Bates et al. 2011b; Eatough et al. 2021; Torne et al. 2021; Suresh et al. 2022), which is possibly due to limited sensitivity (the flux densities of pulsars will be low at high frequencies due to their steep radio spectra) and insufficient sky coverage (a small beam size at high frequency makes it hard to tile the sky efficiently). With new high-frequency pulsar surveys, such as MMGPS at *S* band (1.7–3.5 GHz), more scattered pulsars are expected to be discovered (Padmanabh et al. 2023). To roughly quantify this, we used `PsRPopPy` (Bates et al. 2014)²¹ to model the MSP and normal pulsar populations. We found that $\sim 20\%$ ($\sim 5\%$) of MSPs (normal pulsars) could be missed in pulsar surveys at 1.4 GHz (assuming the sensitivity to be ~ 0.1 mJy) due to scattering (i.e., a scattering timescale longer than the period). When we change the central frequency to 3 GHz, $\sim 70\%$ of pulsars will be undetectable due to the lower flux density (assuming that the sensitivities for 1.4 and 3 GHz surveys are both 0.1 mJy), but $\sim 70\%$ (90%) of previously undiscovered MSPs (normal pulsars) will be visible to the 3 GHz survey, though the computational cost could be prohibitively expensive due to the need to search for a large number of pointings.

The prospects for new pulsar discovery in the imaging domain are promising with the development of new radio continuum surveys, including the GLEAM Extended Survey (Hurley-Walker et al. 2022), LoTSS (Shimwell et al. 2017), RACS (McConnell et al. 2020; Duchesne et al. 2023), EMU with ASKAP (Norris et al. 2011, 2021), the Karl G. Jansky Very Large Array (VLA) Sky Survey (Lacy et al. 2020), and The HUNT for Dynamic and Explosive Radio transients with MeerKAT (Fender et al. 2016) survey. For ASKAP surveys, we considered shallow surveys (with ~ 12 minutes integration time achieving a typical detection threshold of ~ 1.5 mJy) and deep surveys (with ~ 10 hr integration time achieving a typical detection threshold of ~ 50 μ Jy) and quantified the potential new detections with `PsRPopPy` (Bates et al. 2014). We expected to detect four (eight) highly scattered²² MSPs (normal pulsars) in shallow surveys, and 483 (600) in deep surveys. Assuming $\sim 10\%$ of pulsars are detected with circularly polarized emission (e.g., Johnston & Kerr 2018), the number of highly scattered MSPs (normal pulsars) that can be detected via circular polarization searches alone with ASKAP is expected to be one (one) for shallow surveys and 48 (60) for deep surveys. It is unlikely for shallow surveys to discover a large number of highly scattered pulsars with circular polarization searches, but using deep surveys or stacking several shallow surveys can potentially discover a handful of new scattered pulsars. Besides circular polarization searches, other image-domain techniques, such as searching for steep-spectrum sources, high-energy source (e.g., X-ray and γ -ray) associations, and potential SNR (candidate) associations, can also be used in discovering extremely scattered pulsars.

5. Conclusions

We discovered a young, highly scattered pulsar PSR J1032–5804 in the Galactic plane in a search for circularly polarized sources as part of the ongoing ASKAP-VAST survey. The pulsar has a period of 78.7 ms and a DM of 819 ± 4 pc cm⁻³. The long scattering timescale $\tau_{1\text{ GHz}} \approx 3.84$ s makes it the third most scattered pulsar known and also explains the nondetection in previous pulsar surveys, despite its high flux density. Besides circular polarization, linear polarization emission was also detected in the follow-up observations with Murriyang/Parkes. The pulsar has an RM of -2000 ± 1 rad m⁻². Though the measured RM is among the highest RMs detected, it is consistent with the general RM–DM trend and also the Galactic large-scale magnetic field model (e.g., Han et al. 2018).

PSR J1032–5804 is young, with a characteristic age of 34.6 kyr. No X-ray emission was detected in Swift observations, which gives an upper limit to the 0.5–8 keV X-ray luminosity of $1.6 \times 10^{32} d_5^2$ erg s⁻¹. The ratio of the X-ray luminosity to the spindown luminosity is lower than many young pulsars, but is still consistent with the tail of the population. Further deeper X-ray observations may be able to constrain any X-ray emission from the pulsar itself, the PWN, or the SNR shell. ATCA observations combined with archival ASKAP observations revealed that PSR J1032–5804 is a potential GPS source, which suggested strong absorption along the line of sight. A preliminary analysis in this work based on the surrounding extended radio emission and the pulsar radio spectrum may infer the existence of the PWN or SNR. Further observations to measure the SED of the pulsar itself and the spectral map of the extended emission will be useful to understand its local environment and hence probe the properties of the interstellar medium in the vicinity of the pulsar.

This discovery highlights the possibility of discovering new pulsars (especially extreme ones) from continuum images. We can identify more highly scattered pulsars like PSR J1032–5804 with the high-sensitivity and good-resolution data from the ongoing ASKAP surveys. In the future, with the construction of next-generation radio telescopes such as the Square Kilometre Array, the Deep Synoptic Array, and the Next-generation VLA, imaging-domain searches will become a more powerful tool for discovering extreme pulsars (e.g., highly accelerated, highly scattered, and highly intermittent) that are hard to find via traditional surveys.

Acknowledgments

We thank an anonymous referee for helpful comments. We thank Marcus Lower and Apurba Bera for useful discussions. We thank Jackson Taylor and Scott Ransom for help with Algorithmic Pulsar Timing. R.S. is supported by NSF grant AST-1816904. D.K. is supported by NSF grants AST-1816492 and AST-1816904. A.A. is supported by NSF grant AST-1816492. N.H.-W. is the recipient of an Australian Research Council Future Fellowship (project number FT190100231). This scientific work uses data obtained from Inyarrimanha Ilgari Bundara/the Murchison Radio-astronomy Observatory. We acknowledge the Wajarri Yamaji People as the Traditional Owners and native title holders of the Observatory site. CSIRO's ASKAP radio telescope is part of the Australia Telescope National Facility (<https://ror.org/05qajvd42>). The operation of ASKAP is funded by the Australian Government with support from the National Collaborative Research

²¹ <https://github.com/samb8s/PsRPopPy>











²² Here we only considered the pulsars that are undetectable with a 1.4 GHz pulsar survey. Some of the pulsars discussed below are expected to be detected in a 3 GHz pulsar survey as well.

Infrastructure Strategy. ASKAP uses the resources of the Pawsey Supercomputing Research Centre. The establishment of ASKAP, Inyarrimanha Ilgari Bundara, the CSIRO Murchison Radio-astronomy Observatory, and the Pawsey Supercomputing Research Centre are initiatives of the Australian Government, with support from the Government of Western Australia and the Science and Industry Endowment Fund. The Parkes radio telescope is part of the Australia Telescope National Facility, which is funded by the Australian Government for operation as a National Facility managed by CSIRO. We acknowledge the Wiradjuri people as the Traditional Owners of the Observatory site. The Australia Telescope Compact Array is part of the Australia Telescope National Facility (<https://ror.org/05qajvd42>), which is funded by the Australian Government for operation as a National Facility managed by CSIRO. We acknowledge the Gomeri people as the Traditional Owners of the Observatory site. This paper includes archived data obtained through the CSIRO ASKAP Science Data Archive, CASDA (<http://data.csiro.au>). This research has made use of the NASA/IPAC Infrared Science Archive, which is funded by the National Aeronautics and Space Administration and operated by the California Institute of Technology. Based on data products from observations made with ESO Telescopes at the La Silla Paranal Observatory under program ID 177.D-3023, as part of the VST Photometric H α Survey of the Southern Galactic Plane and Bulge (VPHAS+; www.vphas.eu).

Facilities: ASKAP, IRSA, Parkes, Swift (XRT), WISE (<https://www.ipac.caltech.edu/doi/irsa/10.26131/IRSA153>), ATCA, VST.

Software: APTB (Taylor et al. 2023), astropy (Astropy Collaboration et al. 2013, 2018), PINT (Luo et al. 2021), PSRCHIVE (Hotan et al. 2004), PsrPopPy (Bates et al. 2014), Pulsar Survey Scraper (Kaplan 2022), PyGEDM (Price et al. 2021), reproject (Robitaille et al. 2020), swarp (Bertin et al. 2002).

ORCID iDs

Ziteng Wang  <https://orcid.org/0000-0002-2066-9823>
 David L. Kaplan  <https://orcid.org/0000-0001-6295-2881>
 Rahul Sengar  <https://orcid.org/0000-0002-9409-3214>
 Emil Lenc  <https://orcid.org/0000-0002-9994-1593>
 Andrew Zic  <https://orcid.org/0000-0002-9583-2947>
 Akash Anumarlapudi  <https://orcid.org/0000-0002-8935-9882>
 B. M. Gaensler  <https://orcid.org/0000-0002-3382-9558>
 Natasha Hurley-Walker  <https://orcid.org/0000-0002-5119-4808>
 Tara Murphy  <https://orcid.org/0000-0002-2686-438X>
 Yuanming Wang  <https://orcid.org/0000-0003-0203-1196>

References

- Abbate, F., Noutsos, A., Desvignes, G., et al. 2023, *MNRAS*, 524, 2966
 Aharonian, F., Akhperjanian, A. G., Aye, K. M., et al. 2005, *Sci*, 307, 1938
 Aharonian, F., Akhperjanian, A. G., Bazer-Bachi, A. R., et al. 2006, *ApJ*, 636, 777
 Anumarlapudi, A., Ehlke, A., Jones, M. L., et al. 2023, *ApJ*, 956, 28
 Astropy Collaboration, Price-Whelan, A. M., Sipőcz, B. M., et al. 2018, *AJ*, 156, 123
 Astropy Collaboration, Robitaille, T. P., Tollerud, E. J., et al. 2013, *A&A*, 558, A33
 Backer, D. C. 1970, *Natur*, 228, 42
 Backer, D. C., Kulkarni, S. R., Heiles, C., Davis, M. M., & Goss, W. M. 1982, *Natur*, 300, 615
 Bates, S. D., Bailes, M., Bhat, N. D. R., et al. 2011a, *MNRAS*, 416, 2455
 Bates, S. D., Johnston, S., Lorimer, D. R., et al. 2011b, *MNRAS*, 411, 1575
 Bates, S. D., Lorimer, D. R., Rane, A., & Swiggum, J. 2014, *MNRAS*, 439, 2893
 Bates, S. D., Lorimer, D. R., & Verbiest, J. P. W. 2013, *MNRAS*, 431, 1352
 Bertin, E., Mellier, Y., Radovich, M., et al. 2002, in ASP Conf. Ser. 281, Astronomical Data Analysis Software and Systems XI, ed. D. A. Bohlender, D. Durand, & T. H. Handley (San Francisco, CA: ASP), 228
 Bhat, N. D. R., Cordes, J. M., Camilo, F., Nice, D. J., & Lorimer, D. R. 2004, *ApJ*, 605, 759
 Bowman, J. D., Cairns, I., Kaplan, D. L., et al. 2013, *PASA*, 30, e031
 Broderick, J. W., Fender, R. P., Breton, R. P., et al. 2016, *MNRAS*, 459, 2681
 Brogan, C. L., Gaensler, B. M., Gelfand, J. D., et al. 2005, *ApJL*, 629, L105
 Burrows, D. N., Hill, J. E., Nousek, J. A., et al. 2005, *SSRv*, 120, 165
 Camilo, F., Ransom, S. M., Gaensler, B. M., & Lorimer, D. R. 2009, *ApJL*, 700, L34
 Camilo, F., Ransom, S. M., Halpern, J. P., & Roshi, D. A. 2021, *ApJ*, 917, 67
 Condon, J. J., Kaplan, D. L., & Terzian, Y. 1999, *ApJS*, 123, 219
 Condon, J. J., & Ransom, S. M. 2016, *Essential Radio Astronomy* (Princeton, NJ: Princeton Univ. Press)
 Cordes, J. M., & Lazio, T. J. W. 1997, *ApJ*, 475, 557
 Cordes, J. M., & Lazio, T. J. W. 2001, *ApJ*, 549, 997
 Cordes, J. M., & Lazio, T. J. W. 2002, arXiv:astro-ph/0207156
 Cordes, J. M., Pidwerbetsky, A., & Lovelace, R. V. E. 1986, *ApJ*, 310, 737
 Cordes, J. M., & Rickett, B. J. 1998, *ApJ*, 507, 846
 Cordes, J. M., Shannon, R. M., & Stinebring, D. R. 2016, *ApJ*, 817, 16
 Cornwell, T., Humphreys, B., Lenc, E., et al. 2011, ASKAP Science Processing, <https://www.atnf.csiro.au/projects/askap/ASKAP-SW-0020.pdf>
 Cutri, R. M., Wright, E. L., Conrow, T., et al. 2013, Explanatory Supplement to the AllWISE Data Release Products
 Dai, S., Johnston, S., Bell, M. E., et al. 2016, *MNRAS*, 462, 3115
 Dembska, M., Kijak, J., Jessner, A., et al. 2014, *MNRAS*, 445, 3105
 Desvignes, G., Eatough, R. P., Pen, U. L., et al. 2018, *ApJL*, 852, L12
 Drew, J. E., Gonzalez-Solares, E., Greimel, R., et al. 2014, *MNRAS*, 440, 2036
 Duchesne, S. W., Thomson, A. J. M., Pritchard, J., et al. 2023, *PASA*, 40, e034
 Dzub, S., Loinard, L., & Rodríguez, L. F. 2010, *RMxAA*, 46, 153
 Dzub, S. A., Rodríguez, L. F., Karuppusamy, R., Loinard, L., & Medina, S. N. X. 2018, *ApJ*, 866, 100
 Eatough, R. P., Torne, P., Desvignes, G., et al. 2021, *MNRAS*, 507, 5053
 Fender, R., Woudt, P. A., Corbel, S., et al. 2016, in Proc. of MeerKAT Science: On the Pathway to the SKA, ed. Russ Taylor et al., 13
 Gaensler, B. M., Manchester, R. N., & Green, A. J. 1998, *MNRAS*, 296, 813
 Gaensler, B. M., & Slane, P. O. 2006, *ARA&A*, 44, 17
 Gehrels, N., Chincarini, G., Giommi, P., et al. 2004, *ApJ*, 611, 1005
 Gotthelf, E. V. 2003, *ApJ*, 591, 361
 Gotthelf, E. V., & Halpern, J. P. 2009, *ApJL*, 700, L158
 Green, D. A. 2019, *JApA*, 40, 36
 Halpern, J. P., Gotthelf, E. V., & Camilo, F. 2012, *ApJL*, 753, L14
 Han, J. L., Manchester, R. N., van Straten, W., & Demorest, P. 2018, *ApJS*, 234, 11
 Hartman, J. M., Patruno, A., Chakrabarty, D., et al. 2008, *ApJ*, 675, 1468
 He, C., Ng, C. Y., & Kaspi, V. M. 2013, *ApJ*, 768, 64
 Helfand, D. J., Gotthelf, E. V., Halpern, J. P., et al. 2007, *ApJ*, 665, 1297
 Hobbs, G., Manchester, R. N., Dunning, A., et al. 2020, *PASA*, 37, e012
 Hotan, A. W., Bunton, J. D., Chippendale, A. P., et al. 2021, *PASA*, 38, e009
 Hotan, A. W., van Straten, W., & Manchester, R. N. 2004, *PASA*, 21, 302
 Hurley-Walker, N., Callingham, J. R., Hancock, P. J., et al. 2017, *MNRAS*, 464, 1146
 Hurley-Walker, N., Galvin, T. J., Duchesne, S. W., et al. 2022, *PASA*, 39, e035
 Johnston, S., & Kerr, M. 2018, *MNRAS*, 474, 4629
 Johnston, S., Sobey, C., Dai, S., et al. 2021, *MNRAS*, 502, 1253
 Johnston, S., Taylor, R., Bailes, M., et al. 2008, *ExA*, 22, 151
 Kaplan, D. L., 2022 PSS: Pulsar Survey Scraper, Astrophysics Source Code Library, ascl:2210.001
 Kaplan, D. L., Dai, S., Lenc, E., et al. 2019, *ApJ*, 884, 96
 Kargaltsev, O., Durant, M., Pavlov, G. G., & Garmire, G. 2012, *ApJS*, 201, 37
 Kargaltsev, O., & Pavlov, G. G. 2008, in AIP Conf. Ser. 983, 40 Years of Pulsars: Millisecond Pulsars, Magnetars and More, ed. C. Bassa et al. (Melville, NY: AIP), 171
 Keane, E. F., Barr, E. D., Jameson, A., et al. 2018, *MNRAS*, 473, 116
 Keith, M. J., Jameson, A., van Straten, W., et al. 2010, *MNRAS*, 409, 619
 Khan, S., Pandian, J. D., Lal, D. V., et al. 2022, *A&A*, 664, A140
 Kijak, J., Basu, R., Lewandowski, W., & Rożko, K. 2021, *ApJ*, 923, 211

- Kijak, J., Lewandowski, W., Maron, O., Gupta, Y., & Jessner, A. 2011, *A&A*, **531**, A16
- Kramer, M., Lyne, A. G., O'Brien, J. T., Jordan, C. A., & Lorimer, D. R. 2006, *Sci*, **312**, 549
- Lacy, M., Baum, S. A., Chandler, C. J., et al. 2020, *PASP*, **132**, 035001
- Lee, H. G., Moon, D. S., Koo, B. C., et al. 2013, *ApJ*, **770**, 143
- Lenc, E., Murphy, T., Lynch, C. R., Kaplan, D. L., & Zhang, S. N. 2018, *MNRAS*, **478**, 2835
- Lewandowski, W., Kowalińska, M., & Kijak, J. 2015a, *MNRAS*, **449**, 1570
- Lewandowski, W., Rożko, K., Kijak, J., & Melikidze, G. I. 2015b, *ApJ*, **808**, 18
- Li, X. H., & Han, J. L. 2003, *A&A*, **410**, 253
- Lorimer, D. R., & Kramer, M. 2012, *Handbook of Pulsar Astronomy* (Cambridge: Cambridge Univ. Press)
- Lower, M. E., Shannon, R. M., Johnston, S., & Bailes, M. 2020, *ApJL*, **896**, L37
- Luo, J., Ransom, S., Demorest, P., et al. 2021, *ApJ*, **911**, 45
- Lyne, A. G., Manchester, R. N., Lorimer, D. R., et al. 1998, *MNRAS*, **295**, 743
- Manchester, R. N., Hobbs, G. B., Teoh, A., & Hobbs, M. 2005, *AJ*, **129**, 1993
- Manchester, R. N., Lyne, A. G., Camilo, F., et al. 2001, *MNRAS*, **328**, 17
- McConnell, D., Hale, C. L., Lenc, E., et al. 2020, *PASA*, **37**, e048
- Murphy, T., Chatterjee, S., Kaplan, D. L., et al. 2013, *PASA*, **30**, e006
- Murphy, T., Kaplan, D. L., Stewart, A. J., et al. 2021, *PASA*, **38**, e054
- Norris, R. P., Hopkins, A. M., Afonso, J., et al. 2011, *PASA*, **28**, 215
- Norris, R. P., Marvil, J., Collier, J. D., et al. 2021, *PASA*, **38**, e046
- Noutsos, A., Sobey, C., Kondratiev, V. I., et al. 2015, *A&A*, **576**, A62
- O'Brien, J. T., Johnston, S., Kramer, M., et al. 2008, *MNRAS Lett.*, **388**, L1
- Padmanabh, P. V., Barr, E. D., Sridhar, S. S., et al. 2023, *MNRAS*, **524**, 1291
- Posselt, B., Karastergiou, A., Johnston, S., et al. 2023, *MNRAS*, **520**, 4582
- Price, D. C., Flynn, C., & Deller, A. 2021, *PASA*, **38**, e038
- Pritchard, J., Murphy, T., Zic, A., et al. 2021, *MNRAS*, **502**, 5438
- Rajwade, K., Lorimer, D. R., & Anderson, L. D. 2016, *MNRAS*, **455**, 493
- Ransom, S. M. 2001, PhD thesis, Harvard Univ.
- Rickett, B. J. 1970, *MNRAS*, **150**, 67
- Rickett, B. J. 1977, *ARA&A*, **15**, 479
- Ridolfi, A., Gautam, T., Freire, P. C. C., et al. 2021, *MNRAS*, **504**, 1407
- Robitaille, T., Deil, C., & Ginsburg, A., 2020 reprojet: Python-based astronomical image reprojection, Astrophysics Source Code Library, ascl:2011.023
- Romani, R. W., Narayan, R., & Blandford, R. 1986, *MNRAS*, **220**, 19
- Rose, K., Pritchard, J., Murphy, T., et al. 2023, *ApJL*, **951**, L43
- Sengar, R., Bailes, M., Balakrishnan, V., et al. 2023, *MNRAS*, **522**, 1071
- Sett, S., Bhat, N. D. R., Sokolowski, M., & Lenc, E. 2023, *PASA*, **40**, e003
- Shabala, S. S., Ellingsen, S. P., Kurtz, S. E., & Forbes, L. K. 2006, *MNRAS*, **372**, 457
- Shimwell, T. W., Röttgering, H. J. A., Best, P. N., et al. 2017, *A&A*, **598**, A104
- Sieber, W. 1973, *A&A*, **28**, 237
- Sobey, C., Bassa, C. G., O'Sullivan, S. P., et al. 2022, *A&A*, **661**, A87
- Stovall, K., Lynch, R. S., Ransom, S. M., et al. 2014, *ApJ*, **791**, 67
- Suresh, A., Cordes, J. M., Chatterjee, S., et al. 2022, *ApJ*, **933**, 121
- Taylor, J., Ransom, S., & Padmanabh, P. V. 2023, arXiv:2310.10800
- Torne, P., Desvignes, G., Eatough, R. P., et al. 2021, *A&A*, **650**, A95
- Ubertini, P., Bassani, L., Malizia, A., et al. 2005, *ApJL*, **629**, L109
- Wang, Y., Murphy, T., Kaplan, D. L., et al. 2022, *ApJ*, **930**, 38
- Wayth, R. B., Lenc, E., Bell, M. E., et al. 2015, *PASA*, **32**, e025
- Weisberg, S. 2005, *Applied Linear Regression* (New York: Wiley)
- Yao, J. M., Manchester, R. N., & Wang, N. 2017, *ApJ*, **835**, 29